Progress In Electromagnetics Research, Vol. 136, 1–16, 2013

NOVEL COMPACT WAVEGUIDE DUAL CIRCULAR POLARIZER

Chao Chang[1, 2, 4, *], Sami Tantawi[1], Sarah Church[2, 3], Jeffery Neilson[1], and Patricia V. Larkoski[2, 3]

[1]SLAC National Accelerator Laboratory, Stanford University, Stanford, CA 94309, USA

[2]Kavli Institute for Particle Astrophysics & Cosmology, Stanford University, Stanford, CA 94309, USA

[3]Department of Physics, Stanford University, 382 Via Pueblo Mall, Stanford, CA 94305, USA

[4]Department of Engineering Physics, Tsinghua University, Beijing 100084, China

Abstract—A novel type of dual circular polarizer for simultaneously receiving and transmitting right-hand and left-hand circularly polarized waves is developed and tested. It consists of a H-plane T junction of rectangular waveguide, one circular waveguide as an E-plane arm located on top of the junction, and two metallic pins used for matching. The theoretical analysis and design of the three-physical-port and four-mode polarizer were researched by solving Scattering-Matrix of the network and using a full-wave electromagnetic simulation tool. The optimized polarizer has the advantages of a very compact size with a volume smaller than $0.6\lambda^3$, low complexity and manufacturing cost. A couple of the polarizer has been manufactured and tested, and the experimental results are basically consistent with the theories.

1. INTRODUCTION

A circular polarizer is a device to convert a right-hand circular polarization (RHCP) and/or left-hand circular polarization (LHCP) into linearly polarized signals of vertically polarized (VP) and/or horizontally polarized (HP) waves, or is used in a reverse way [1, 2]. The transformation of circular polarization with linear polarization

Received 10 December 2012, Accepted 7 January 2013, Scheduled 11 January 2013

* Corresponding author: Chao Chang (chang@slac.stanford.edu).

is generally realized by loading the discontinuities of a stepped-septum [3–8], stepped-corrugations [9–12], grooves [13] and loaded dielectrics [14, 15].

In this paper, we developed a new compact circular polarizer. This work is motivated by the development of instrumentations for the next generation experiments detecting the polarization of the cosmic microwave background (CMB) in order to understand the very early Universe [16]. The incident circularly polarized radiations are received by an array of circular feed horns, converted, and then separated into two rectangular waveguides for respective analysis. In order to build an instrument with hundreds of array elements, each unit needs to be small to allow for close-packing. Other kind of circular polarizers such as microstrip polarizer [17–23] also have the disadvantage of narrow bandwidth and low efficiency due to losses of conductor, dielectric and surface wave.

For a dual circular polarizer, two devices are usually needed [2, 13]: A circular polarizer to convert RHCP and LHCP radiation into respective VP and HP waves, and an ortho-mode transducer (OMT) to split the VP and HP waves into two separate waveguide ports. The polarizer together with the OMT forms a sub-system with three physical interface ports, whose total size is relatively large. In Ref. [13], a dual circular polarizer consisting of a circular polarizer realized by a pair of large grooves and an OMT by two rectangular waveguides with a perpendicular H-plane junction was designed. In this paper, we propose and test a new more compact dual circular polarizer, whose generation and mechanism is significantly different from the previous one. In more details, the isolation of two rectangular ports and generating the RHCP and LHCP in the circular port are realized by the H-plane stub and two central pins. The network and S-matrix for the present polarizer will be explained in Sections 2 and 3. The manufacture for the present dual circular polarizer is simpler than that for the previous one, illustrated in Section 4. The designed frequency range of the polarizer is in the Ka-band, and it should be emphasized that this device can be scaled to different frequency bands.

2. ANALYSIS AND OPTIMIZATION OF A TURNSTILE POLARIZER

Consider a symmetric structure shown in Fig. 1, consisting of a turnstile of rectangular waveguides coupled with a circular waveguide in the E plane. This structure has five ports (four rectangular ports labeled Port 1, Port 3, Port 4 and Port 5, and one circular labeled Port 2) and six modes (identified as Port N:M, where N is the port

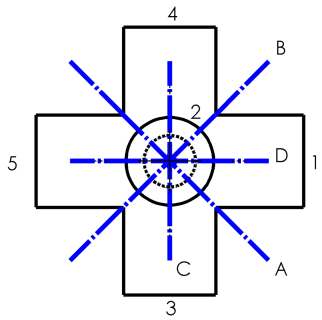

Figure 1. A symmetric turnstile of rectangular waveguides coupled to a circular waveguide.

number and M is the mode number associated with Port N). There are four symmetric planes: diagonal planes A and B, and horizontal and vertical planes C and D. This structure is conventionally used as a turnstile OMT [24–28]. However, we will demonstrate that the S-parameter for the OMTs described in Ref. [24–28] is significantly different from that for the design presented here. The design goal of the Scattering-Matrix for the six modes is the following:

$$S = \frac{1}{2}\begin{pmatrix} 0 & \sqrt{2} & 0 & 1 & 1 & 0 \\ \sqrt{2} & 0 & 0 & 0 & 0 & -\sqrt{2} \\ 0 & 0 & 0 & \sqrt{2} & -\sqrt{2} & 0 \\ 1 & 0 & \sqrt{2} & 0 & 0 & 1 \\ 1 & 0 & -\sqrt{2} & 0 & 0 & 1 \\ 0 & -\sqrt{2} & 0 & 1 & 1 & 0 \end{pmatrix} \tag{1}$$

If incident power from only Port 1, corresponding to $\mathbf{a}_1 = [1, 0, 0, 0, 0, 0]^T$, the output vector is $\mathbf{b}_1 = \mathbf{S} \cdot \mathbf{a}_1 = [0, \sqrt{2}, 0, 1, 1, 0]^T/2$, implying that 1/2 power is excited at Port 2; two TE_{10} modes with 1/4 equal power and equivalent phase are generated at Ports 3 and 4; and Port 5 is isolated. For input power from four rectangular ports with equal amplitude but with specific incident phases, if line A is an electric boundary and B is a magnetic boundary, then the equivalent input column vector is $\mathbf{a}_2 = [1, 0, 0, -1, 1, -1]^T/2$, and the output vector is $\mathbf{b}_2 = \mathbf{S} \cdot \mathbf{a}_2 = [0, \sqrt{2}, \sqrt{2}, 0, 0, 0]^T/2$, if line A is an magnetic boundary and B is a electric boundary, then the equivalent input column vector is $\mathbf{a}_3 = [1, 0, 0, 1, -1, -1]^T/2$, and the output vector is still $\mathbf{b}_2 = \mathbf{S} \cdot \mathbf{a}_3 = [0, \sqrt{2}, \sqrt{2}, 0, 0, 0]^T/2$, which means that there is equal excitation of modes Port 2:1 and Port 2:2, and no reflection in any rectangular port. If both A and B are magnetic boundaries, then the input and output vector are ei-

ther the same $\mathbf{a}_3 = [1, 0, 0, 1, 1, 1]^T/2$, there is no mode excited in the circular waveguide when the higher order mode (i.e., TM_{01}) is cutoff in the circular waveguide. Similarly, there is no mode excited if both A and B are electric boundaries. By assigning A as an electric boundary and B as a magnetic boundary, the turnstile junction is decomposed to four units, and a quarter structure consisting of Port 1 and 1/4 of Port 2 is obtained. By using the 3-D electromagnetic simulation tool HFSS [29], the quarter structure is optimized, whose S parameter can be matched by adding two metallic posts to the center and adjusting their heights and diameters. The matched quarter structure supplies a range of parameters of the pins to help to realize the whole S-Matrix in HFSS simulation. The finally optimized field distribution and S parameters are shown in Fig. 2.

Figures 2(a) and (b) show that, when the structure is matched and fed with unit power in Port 1, TE_{11} mode Port 2:1 polarized along the incident rectangular waveguide with -3 dB power is excited in the circular waveguide Port 2; two TE_{10} modes with power of -6 dB and equivalent phase are equally generated at the neighbor Ports 3 and 4; the opposite Port 5 is isolated; and there is no coupling to the TE_{11} mode Port 2:2 ($S_{1,2:2} < -50$ dB in the frequencies, and not shown in Fig. 2(b)). As a comparison, take an example, the turnstile OMT in Ref. [27] is as illustrated in Fig. 3(a). For an incident wave at Port 1, one-half power is excited in the circular port, as shown in Figs. 3(b) and (c), however, the opposite port is not isolated, there are strong reflection back, and the neighbor ports have $< 1/4$ power. The S-parameters for the turnstile OMT in Ref. [24–28] are also found to be different from the structure presented here.

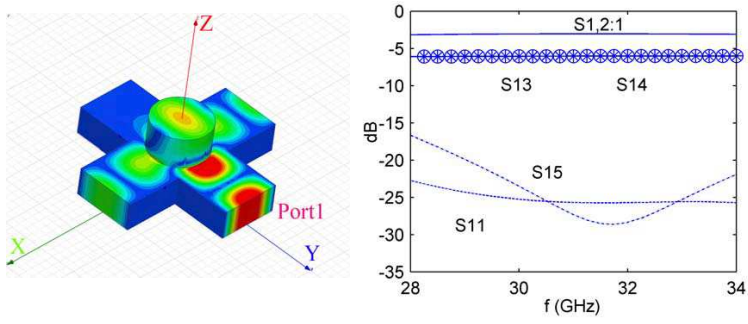

(a) (b)

Figure 2. (a) The transient surface electric field and (b) S parameters of the 5-port symmetric structure; 'o' and '*' respectively for S_{13} and S_{14} (Wave incidence from port 1 with a unit power).

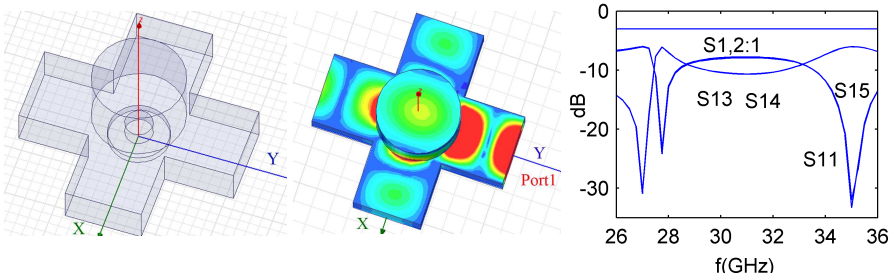

(a) (b) (c)

Figure 3. The Turnstile OMT published in Ref. [27], (a) structure with two posts, (b) transient surface field for incident wave at Port 1 and (c) S-parameters ($S_{1,2:1} \sim -3\,\text{dB}$, S_{13} and S_{14} have overlapped curves, S_{11} and S_{15} have overlapped curves).

Now, we discuss how the polarizer can be realized. When incident wave E_0 is fed in Port 1, the excited field $E_0/2$ towards Port 3 and Port 4 are the same with equal phases, shown in Fig. 4(a). It should be emphasized that the phase of the incident wave at the central area determines the phases of the excited waves in adjacent ports and Port 2. For instance, and the incident wave from Port 3 with 0° phase and field $E_0/2$ at the central area excites the neighbor Port 5 and Port 1 with transient electric vector direction out of page and field $E_0/4$, and electric vector of mode Port 2:2 towards Port 4 with field $\sqrt{2}E_0/4$, shown in Fig. 4(b); incident wave from Port 4 with 180° phase and field $-E_0/2$ at the central area excites the neighbor Port 5 and Port 1 with transient electric vector direction into the page and field $-E_0/4$, and electric vector of mode Port 2:2 also towards Port 4 with field $\sqrt{2}E_0/4$, illustrated as Fig. 4(c), The question is how could the Port 3 and Port 4 have 180° phase difference at the central area? By placing a short on arms 3 and 4, and adjusting their phase length difference to be equal to $(2n+1)\lambda_g/4$, where n is an nonnegative integer, when the waves reflected from the shorted Ports of 3 and 4 arrives at the central area, they will have a phase difference of 180°, which means two opposite incident phases. Consequently, the Port 2:2 respectively excited by the shorted Ports 3 and 4 are summed to $\sqrt{2}/2E_0$, and the TE_{10} modes generated towards Port 1 and 5 are fully cancelled. Thus, two orthogonal TE_{11} modes with equal amplitude are excited by the structure.

When the phase difference of two orthogonal mode Port 2:1 and Port 2:2 is 90° or −90°, the turnstile polarizer is realized, and the optimized dimensions are illustrated in Table 1, and the S-parameter

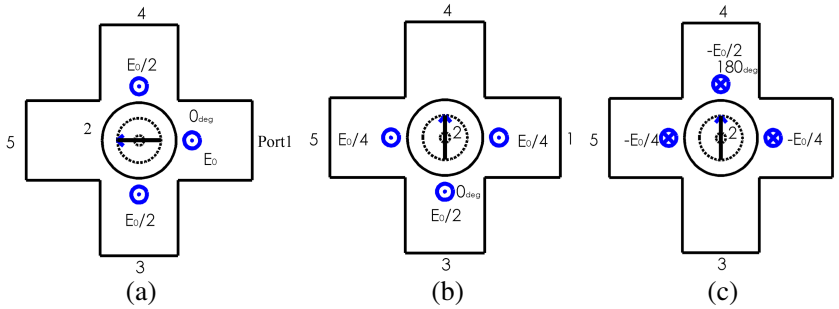

Figure 4. The excited modes and the corresponding phases for different incident ports. (a) Port 1 fed in with 0° wave. (b) Port 3 with 0° wave. (c) Port 4 fed in with 180° wave. The circled cross and circled dot symbols respectively represents transient vector of the electric field in and out of the page.

Table 1. The optimized parameter for a turnstile polarizer (in unit of mm).

Rectangular waveguide		Circular waveguide	Length difference L_{arm4}-L_{arm3}	Cylinder Pins			
Width W_r	Height H_r	Radius R_c	$(2n+1)\lambda_g/4$ L_{arm3} not close to zero	Radius R_1	Height Z_1	Radius R_2	Height Z_2
7.6	3.455	3.6		2.12	1.05	0.48	3.56

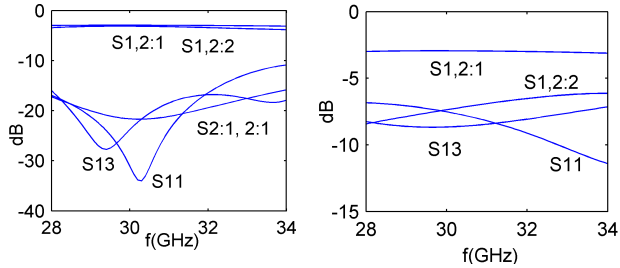

Figure 5. S parameters of the turnstile polarizer for the arm 3 length of (a) 5.6 mm and (b) 0 mm.

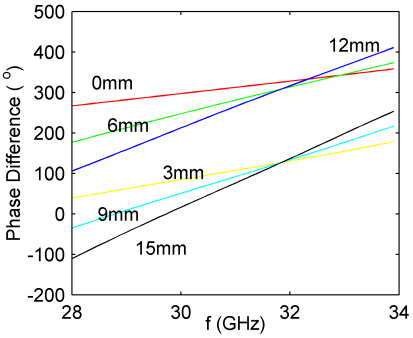

Figure 6. Variation of phase difference of TE_{11} modes 1 and 2 with arm lengths L_3.

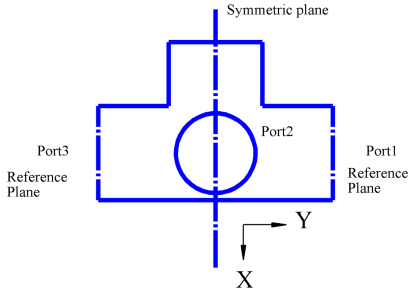

Figure 7. Schematic of the dual circular polarizer.

is shown in Fig. 5(a). A turnstile polarizer was researched firstly in Ref. [30]. However, it did not give any theoretical or experimental S-parameters. Only far field radiation patterns were recorded, and there was no information on its bandwidth. The physics of how the polarizer realized was not explained clearly. Actually, the phase response on frequency influences the bandwidth of the polarizer, which will be shown in the following paragraph.

The phase of the mode Port 2:2 depends on the arm lengths L_3 and L_4 of the branches at Ports 3 and 4. The phases φ_3 and φ_4 of the reflected wave at the entrance of the central area is $\varphi_{3,4} \sim 2\beta L_{3,4}$, where β is the propagation constant. Thus, the phase of excited the mode Port 2:2 is varied for different lengths $L_{3,4}$, and the phase difference of two orthogonal mode Port 2:1 and Port 2:2 is varied with branch lengths, as shown in Fig. 6. It is found that the slope of the phase difference decreases when the arm length shortens and it reaches the minimum when the arm 3 vanishes and the arm 4 is $1/4\lambda_g$ long. This is because the propagation constant β depends on frequency, $\varphi_{3,4}(f, L_{3,4}) \sim 2\beta(f)L_{3,4}$, and the longer $L_{3,4}$, the larger the variation range of $\varphi_{3,4}$ for different frequencies. Thus, the slope of phase variation of TE_{11} mode 2 decreases with shortening the arm length. Consequently, the profile of the circular polarizer has become an H-type T junction of rectangular waveguide, with a shorted H-plane arm of a $1/4\lambda_g$ long, and one E-plane circular waveguide located on top. However, when the arm 3 trends towards zero and the arm 4 is close to $1/4\lambda_g$, the evanescent wave excited at port 3 and port 4 will significantly disturb the electric boundary, hence, the center pins used to match the S-Matrix for a Turnstile polarizer becomes

mismatched, as illustrated the S parameters in Fig. 5(b), compared with the matched one in Fig. 5(a). Thus, using the five ports with six modes to analyze the new H-type T junction polarizer is not suitable any more. Consequently, the paper in Ref. [30] could not make one arm close to zero. A theory for the dual circular polarizer with three physical ports and four modes should be studied.

3. THE FOUR-PORT DUAL CIRCULAR POLARIZER

For the dual circular polarizer with three physical ports and four modes, as illustrated in Fig. 7, its special S-Matrix needs to be researched. There is only one symmetric plane for a non-zero stub-arm length. The eigen-vectors of the S-matrix of the 4-modes network are denoted by a column vector $[a,\, b,\, c,\, d]^T$, where a, b, c, and d are respectively the amplitudes of the wave in port 1, 2:1, 2:2, and 3. The modes Port 2:1 and Port 2:2 are respectively along Y and X axis. Due to the electric and magnetic symmetry with regard to the dashed line, the four eigen-vectors of the S-matrix can be written as $[1,\, b1,\, 0,\, -1]^T$, $[1,\, b2,\, 0,\, -1]^T$, $[1,\, 0,\, c1,\, 1]^T$, and $[1,\, 0,\, c2,\, 1]^T$. Owing to the orthogonal basis of eigenvectors, the dot product of every two eigenvector should be zero, thus, $b1 \times b2 = -2$, and $c1 \times c2 = -2$. It is possible to choose the position of the reference planes in such a way [24] that $b1 = c1 = \sqrt{2}$, and then, $b2 = c2 = -\sqrt{2}$. The normalized orthogonal Matrix of eigenvectors $\mathbf{X}$ is

$$\mathbf{X} = \frac{1}{2}\begin{pmatrix} 1 & 1 & 1 & 1 \\ \sqrt{2} & -\sqrt{2} & 0 & 0 \\ 0 & 0 & \sqrt{2} & -\sqrt{2} \\ -1 & -1 & 1 & 1 \end{pmatrix} \tag{2}$$

Since a 4×4 S-matrix is diagonalizable if and only if the sum of the dimensions of the eigen-spaces is 4. Or, equivalently, if and only if S has 4 linearly independent eigenvectors. Consequently, the S-Matrix of 4-port network can be diagonalizable by the orthogonal eigenvectors Matrix as,

$$\mathbf{S} = \mathbf{X}\begin{pmatrix} \lambda_1 & 0 & 0 & 0 \\ 0 & \lambda_2 & 0 & 0 \\ 0 & 0 & \lambda_3 & 0 \\ 0 & 0 & 0 & \lambda_4 \end{pmatrix}\mathbf{X^{-1}} \tag{3}$$

$\mathbf{X}^{-1}$ is the inverse matrix of $\mathbf{X}$, and λ_i, $i = 1, 2, 3$, and 4 are the

eigen-values of the S-Matrix. By solving the Eq. (3), there is,

$$\mathbf{S}=\frac{1}{4}\begin{pmatrix} \sum\lambda_i & \sqrt{2}\,(\lambda_1-\lambda_2) & \sqrt{2}\,(\lambda_3-\lambda_4) & -\lambda_1-\lambda_2+\lambda_3+\lambda_4 \\ \sqrt{2}\,(\lambda_1-\lambda_2) & 2(\lambda_1+\lambda_2) & 0 & \sqrt{2}\,(\lambda_2-\lambda_1) \\ \sqrt{2}\,(\lambda_3-\lambda_4) & 0 & 2(\lambda_3+\lambda_4) & \sqrt{2}\,(\lambda_3-\lambda_4) \\ -\lambda_1-\lambda_2+\lambda_3+\lambda_4 & \sqrt{2}\,(\lambda_2-\lambda_1) & \sqrt{2}\,(\lambda_3-\lambda_4) & \sum\lambda_i \end{pmatrix} \tag{4}$$

The eigen-values in Eq. (4) can be addressed by realizing the function of the dual circular polarizer. For a wave incident with an unit power at Port 1, $\mathbf{a}_1 = [1, 0, 0, 0]^T$, the output is a circular polarized wave, $\mathbf{b}_1 = \mathbf{S}\cdot\mathbf{a}_1=\sqrt{2}[0, 1, i, 0]/2$. Besides, for equal incident power with the same phase from Port 1 and Port 3, $\mathbf{a}_2 = \sqrt{2}[1, 0, 0, 1]^T/2$, the symmetric plane at Port 2 is equivalent to a magnetic boundary, and only Port 2:2 is excited, corresponding to $\mathbf{b}_2 = \mathbf{S}\cdot\mathbf{a}_2=[0, 0, i, 0]^T$; for equal incident power with 180° phase difference from Port 1 and Port 3, $\mathbf{a}_3 = \sqrt{2}\,[1, 0, 0, -1]^T/2$, the symmetric plane at Port 2 is equivalent to a electric boundary, and only Port 2:1 is excited, corresponding to $\mathbf{b}_3 = \mathbf{S}\cdot\mathbf{a}_3=[0, 1, 0, 0]^T$. From the three input vector $\mathbf{a}_{1,2,3}$, and the corresponding output vector $\mathbf{b}_{1,2,3}$, the eigen-values can be solved in the following equations,

$$\begin{array}{ll} \sum\lambda_i = 0 & \lambda_3+\lambda_4-\lambda_1-\lambda_2 = 0 \\ \lambda_1-\lambda_2 = 2 & \lambda_1+\lambda_2 = 0 \\ \lambda_3-\lambda_4 = 2i & \lambda_3+\lambda_4 = 0 \end{array} \tag{5}$$

By solving Eq. (5), the eigen-values for the dual circular polarizer are $\lambda_1 = 1$, $\lambda_2 = -1$, $\lambda_3 = i$, and $\lambda_4 = -i$. And the Scattering-Matrix in Eq. (4) can be simplified as,

$$\mathbf{S} = \frac{\sqrt{2}}{2}\begin{pmatrix} 0 & 1 & i & 0 \\ 1 & 0 & 0 & -1 \\ i & 0 & 0 & i \\ 0 & -1 & i & 0 \end{pmatrix} \tag{6}$$

This S-matrix in Eq. (6) is the design goal for the dual circular polarizer, which needs the eigen-values to satisfy $\lambda_1 = -\lambda_2$, $\lambda_3 = -\lambda_4$, and $\lambda_1 = i\lambda_3$. The three key conditions can be achieved at the same time by tuning the two center pins and the stub. In more detail, by adjusting the height and radius of the dumpy pin and the slim pin, and the length and width of the stub, the polarizer can be obtained. The eigen-values $\lambda_1 = 1$ and $\lambda_2 = -1$ and the corresponding eigen vectors $[1, \sqrt{2}, 0, -1]^T/2$ and $[1, -\sqrt{2}, 0, -1]^T/2$ are equivalent to the condition that the symmetric plane is equivalent to an electric boundary, which means that physically there are equal amplitude field with a 180° phase difference incident at port 1 and port 3, as illustrated in Fig. 8(a). In this situation, the stub is cutoff and there is only

evanescent wave in the stub, as shown in Fig. 8(b); electric field on the slim pin is very small due to the slim pin located very close to the electric boundary, as shown in Fig. 8(c). In HFSS simulation, by taking the symmetric plane as electric boundary, a two-physical-port and two-mode network is obtained and optimized, instead of studying the four-port polarizer. Thus, by tuning the dumpy pin, the two-port network is matched, and $\lambda_1 = -\lambda_2$ is realized in this situation.

Similarly, the eigen-values $\lambda_3 = i$ and $\lambda_4 = -i$ and the corresponding eigen vectors $[1,\ \sqrt{2},\ 0,\ 1]^T/2$ and $[1,\ -\sqrt{2},\ 0,\ 1]^T/2$ are equivalent to the symmetric plane as an magnetic boundary, which means that physically there are equal amplitude field with the same phase incident at port 1 and port 3, as illustrated in Figs. 9(a) and (b). In HFSS simulation, by using the magnetic symmetric plane, a two-port network is obtained; and by adjusting the slim pin and the width and the length of the stub to realize $\lambda_3 = -\lambda_4$ and $\lambda_1 = i\lambda_3$, the mode Port 2:2 with the equal amplitude of Port 2:1 and a 90° phase difference can be realized. Thus, a circular polarizer wave for this structure is generated with the transient surface field shown in Fig. 10.

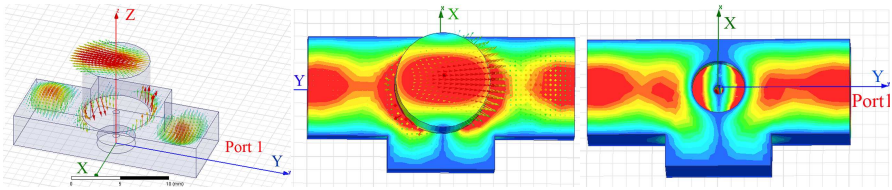

(a) (b) (c)

Figure 8. (a) The vector electric field and complex magnitude of surface field, (b) on top surface, and (c) on bottom for the equivalent symmetric electric boundary.

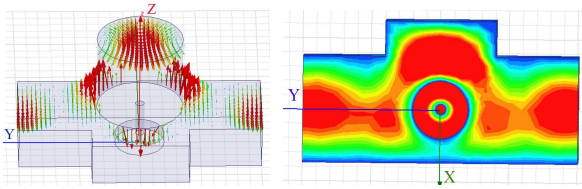

(a) (b)

Figure 9. (a) The vector electric field and (b) complex magnitude on bottom surface for the equivalent symmetric magnetic boundary.

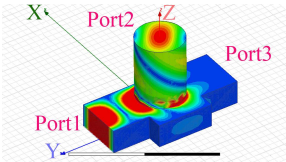

Figure 10. The instantaneous surface field distribution of the optimized circular polarizer.

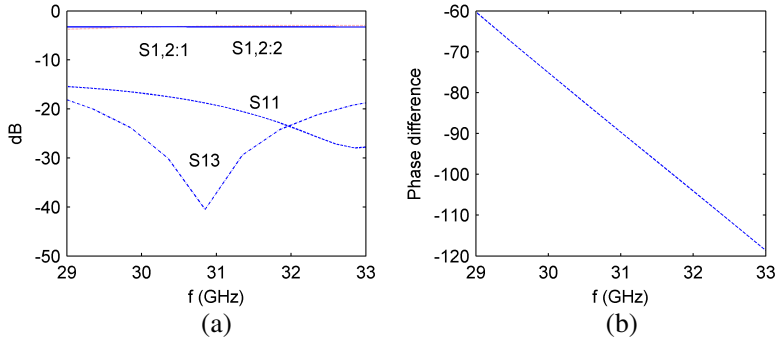

Figure 11. (a) S parameters of the dual polarizer; S_{11} for return loss; $S_{1:2:1}$ and $S_{1:2:2}$ for transition to two orthogonal TE_{11} modes; S_{13} for isolation; (b) Phase difference of two orthogonal TE_{11} modes.

In order to increase the bandwidth, the dependence of propagation constant on frequency should be decreased. This can be achieved by broadening the width of the stub since β for a wider waveguide is less sensitive on frequency. Also, the path for exciting TE_{11} mode 2 is from Port 1 to the stub and then to Port 2, which is longer than the path for generating TE_{11} mode 1, thus, it is always sensitive to frequency. Widening the H-plane arm has the benefit of decreasing the path length for TE_{11} mode 2, effectively reducing the difference between the two path lengths. The optimized S parameters of the polarizer given in Figs. 11(a) and (b) show that the two orthogonal TE_{11} modes have relatively equal -3B amplitude, the isolation and return loss are respectively below -30 dB and -15 dB, and the phase difference between the two TE_{11} modes varies of 60° from 29 GHz to 33 GHz. It should be emphasized that a pure circular wave requires a 90° differential phase between two orthogonal modes. As the frequency increases or decreases from the center frequency, the phase difference moves away from 90°, leading to a decrease in the circularly polarized power. When this structure is used in the reverse way, the input RHCP and LHCP in circular Port 2 is respectively transformed into separated linear polarization in the two rectangular Ports 1 and 3. Thus, this device is a compact dual circular polarizer. Based on the above analysis, finally, the optimized parameter is shown in Table 2, which is also the same data of the manufactured polarizer. Note that the matched stub length $L_s = 2.5$ mm is no long $1/4\lambda_g$, which is 3 mm for stub width $W_s = 8.05$ mm and 3.2 mm for waveguide width $W_r = 7.44$ mm.

4. MANUFACTURE AND TEST

Two pieces of dual circular polarizer with the material of brass have been manufactured, and the split-block design has been used to respectively fabricate the bottom and top block, as illustrated in Fig. 12. The central circular step and pin are accurately built at the bottom block, and the H-plane arm as well as the rectangular and circular waveguides are located at the top block. This compact circular polarizer has an inner volume smaller than $0.6\lambda^3$, and the outer metal block is $0.36\,\text{inch}^3$.

Agilent E8364B PNA Network Analyzer is used to measure the S parameters. In order to measure the return loss and isolation, as shown in Fig. 13(a), two matched terminations are connected with the inputs of one polarizer, two coaxial to WR28 waveguide adapters are linked the inputs of the other polarizer with the VNA, and then, two polarizers are connected back to back with a circular waveguide. The experimental return loss and isolation are basically consistent with the simulation results, as illustrated in Fig. 14.

The second step is to measure the insertion loss of the polarizer. When a linear polarizer wave is incident in Port 1 of the polarizer, a LHCP wave is generated and outputted at the circular Port 2. By

Table 2. The optimized parameter for the compact dual circular polarizer (in unit of mm).

Rectangular waveguide		Stub		Circular waveguide	Cylinder Pins			
W_r	H_r	W_s	L_s	R_c	R_1	Z_1	R_2	Z_2
7.44	3.46	8.05	2.5	3.55	2.02	0.92	0.37	2.85

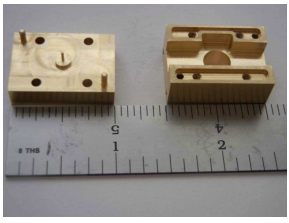

Figure 12. The photograph of the fabricated polarizer.

(a) (b)

Figure 13. (a) Measurement for the return loss and isolation of one polarizer. (b) Measurement for the circular polarization.

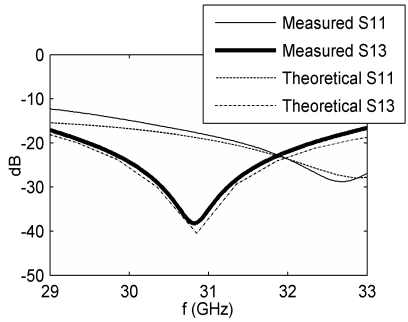

Figure 14. Comparison of the measured and theoretical return loss S_{11} and isolation S_{13}.

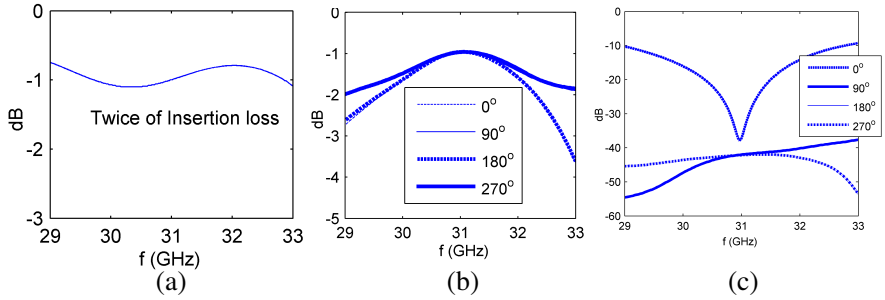

Figure 15. (a) Twice of the insertion loss, (b) the output of one rectangular port and (c) the output of the other rectangular port for back-to-back jointed polarizers by successively rotating one polarizer with 0°, 90°, 180°, and 270°.

placing a short metal plane at the Port 2, the polarization of incident LHCP changes to RHCP after reflection, thus, the Port 3 receives the signal, and the transmission coefficient of one polarizer is shown in Fig. 15(a), where twice of the averaged insertion loss is about −1 dB.

In order to measure the circular polarization, two polarizers are jointed back to back with a commercial circular waveguide plated by gold, one adapter and one load are connected with one polarizer, as illustrated in Fig. 13(b), the output of the LHCP from one polarizer changes to LP after the second polarizer, and further outputs in one rectangular port, with the other rectangular port isolated. Then, by rotating one of the polarizer successively by 0°, 90°, 180°, and 270°, the outputs of one rectangular port are shown in Fig. 15(b) representing the circular polarizer wave, and the output in the other port in Fig. 15(c)

represents the cross polarization. It should be emphasized that the outputs in Fig. 15(b) and (c) are the results from one polarizer jointed to the other polarizer, for a single polarizer, the bandwidth of the output will be higher than those in Figs. 15(b) and (c).

5. CONCLUSIONS

A novel compact waveguide circular polarizer with a three-physical port and a four mode network has been developed. The prototypes of the polarizer have been tested, and the experimental results are consistent with theoretical analysis.

ACKNOWLEDGMENT

This work is supported by Department of Energy contract DE-AC02-76SF00515.

REFERENCES

1. Uher, J., J. Bornemann, and U. Rosenberg, *Waveguide Components for Antenna Feed Systems: Theory and CAD*, Artech House, Norwood, MA, 1993.
2. Bertin, G., B. Piovano, L. Accatino, and M. Mongiardo, "Full-wave design and optimization of circular waveguide polarizers with elliptical irises," *IEEE Trans. Microw. Theory Tech.*, Vol. 50, No. 4, 1077–1083, Apr. 2002.
3. Chen, M. H. and G. N. Tsandoulas, "A wide-band square waveguide array polarizer," *IEEE Trans. Antennas Propagat.*, Vol. 21, 389–391, May 1973.
4. Ege, T. and P. McAndrew, "Analysis of stepped septum polarizers," *Electronic Lett.*, Vol. 21, 1166–1168, Nov. 1985.
5. Piovano, B., G. Bertin, L. Accatino, and M. Mongiardo, "CAD and optimization of compact wide-band septum polarizers," *Eur. Microwave Conf.*, Munich, Germany, 1999.
6. Bornemann, J. and V. A. Labay, "Ridge waveguide polarizer with finite and stepped-thickness septum," *IEEE Trans. Microwave Theory Tech.*, Vol. 43, 1782–1787, Aug. 1995.
7. Zhong, W. Y., B. Li, Q. Y. Fan, and Z. Q. Shen, "X-band compact septum polarizer design," *ICMTCE*, 167–170, May 22–25, 2011.
8. Ihmels, R., U. Papziner, and F. Arndt, "Field theory design of a corrugated septum OMT," *IEEE MTT-S Int. Microwave Symp. Dig.*, 909–912, 1993.

9. Jung, Y. B., "Ka-band polariser structure and its antenna application," *Electronics Letters*, Vol. 45, 931–932, 2009.
10. Eom, S. Y. and Y. B. Korchemkin, "A new comb circular polarizer suitable for millimeter-band application," *ETRI J.*, Vol. 28, No. 5, 656–659, Oct. 2006.
11. Virone, G., R. Tascone, M. Baralis, O. A. Peverini, A. Olivieri, and R. Orta, "A novel design tool for waveguide polarizers," *IEEE Trans. Microwave Theory Tech.*, Part 1, Vol. 53, No. 3, 888–894, Mar. 2005.
12. Virone, G., R. Tascone, O. A. Peverini, G. Addamo, and R. Orta, "Combined-phase-shift waveguide polarizer," *IEEE Microwave and Wireless Components Letters*, Vol. 18, No. 8, 509–511, 2008.
13. Chang, C., S. Church, S. G. Tantawi, P. Voll, M. Sieth, and K. Devaraj, "Theory and experiment of a compact waveguide dual circular polarizer," *Progress In Electromagnetics Research*, Vol. 131, 211–225, 2012.
14. Wang, S. W., C. H. Chien, C. L. Wang, and R. B. Wu, "A circular polarizer designed with a dielectric septum loading," *IEEE Trans. Microwave Theory Tech.*, Vol. 52, 1719–1723, Jul. 2, 2004.
15. Zhang, T. I. and Z. H. Yan, "A Ka dual-band circular waveguide polarizer," *7th Int. Symp. on Antennas, Propagation & EM Theory*, 1–4, Oct. 2006.
16. Kovac, M., E. M. Leitch, C. Pryke, J. E. Carlstrom, N. W. Halverson, and W. L. Holzapfel, "Detection of polarization in the cosmic microwave background using DASI," *Nature*, Vol. 420, 772–787, 2002.
17. Letizia, M., B. Fuchs, C. Zorraquino, J.-F. Zurcher, and J. R. Mosig, "Oblique incidence design of meander-line polarizers for dielectric lens antennas," *Progress In Electromagnetics Research B*, Vol. 45, 309–335, 2012.
18. Heidari, A., M. Heyrani, and M. Nakhkash, "A dual-band circularly polarized stub loaded microstrip patch antenna for GPS applications," *Progress In Electromagnetics Research*, Vol. 92, 195–208, 2009.
19. Masa-Campos, J. L. and F. Gonzalez-Fernandez, "Dual linear/circular polarized plannar antenna with low profile double-layer polarizer of 45± tilted metallic strips for WiMAX applications," *Progress In Electromagnetics Research*, Vol. 98, 221–231, 2009.
20. Sze, J.-Y. and S.-P. Pan, "Design of broadband circularly polarized square slot antenna with a compact size," *Progress In*

Electromagnetics Research, Vol. 120, 513–533, 2011.

21. Wu, G.-L., W. Mu, G. Zhao, and Y.-C. Jiao, "A novel design of dual circularly polarized antenna FED by lstrip," *Progress In Electromagnetics Research*, Vol. 79, 39–46, 2008.
22. Chen, X., G. Fu, S.-X. Gong, Y.-L. Yan, and J. Chen, "Parametric studies on the circularly polarized stacked annular-ring microstrip antenna," *Progress In Electromagnetics Research C*, Vol. 12, 65–77, 2010.
23. Lin, C., F.-S. Zhang, Y. Zhu, and F. Zhang, "A novel three-fed microstrip antenna for circular polarization application," *Journal of Electromagnetic Waves and Applications*, Vol. 24, Nos. 11–12, 1511–1520, 2010.
24. Montgomery, C. G., R. H. Dicke, and E. M. Purce, *Principles of Microwave Circuits*, Boston Technical Lithographers Inc., Lexington, USA, 1963.
25. Aramaki, Y., N. Yoneda, M. Miyazaki, and T. Horie, "Ultra-thin broadband OMT with turnstile junction," *IEEE MTT-S Int. Dig.*, Vol. 1, 47–50, Jun. 2003.
26. Navarrini, A. and R. L. Plambeck, "A turnstile junction waveguide orthomode transducer," *IEEE Trans. Microw. Theory Tech.*, Vol. 54, No. 1, 272–277, Jan. 2006.
27. Pisano, G., et al., "A broadband WR10 turnstile junction orthomode transducer," *IEEE Microwave and Wireless Components Letters*, Vol. 17, 286, 2007.
28. Tribak, A., J. L. Cano, A. Mediavilla, and M. Boussouis, "Octave bandwidth compact turnstile-based orthomode transducer," *IEEE Microwave and Wireless Components Letters*, Vol. 20, No. 10, 539–541, 2008.
29. HFSS, USA, http://www.ansys.com/.
30. Crandell, P. A., "A turnstile polarizer for rain cancellation," *Transactions of the IRE Professional Group on Microwave Theory and Techniques*, Vol. 3, No. 1, 10–15, Jan. 1955.